

Article

Mapping Highland Barley on the Qinghai–Tibet Combing Landsat OLI Data and Object-Oriented Classification Method

Weidong Ma ¹, Wei Jia ¹, Peng Su ¹, Xingyun Feng ², Fenggui Liu ^{1,3} and Jing'ai Wang ^{2,3,*}

- ¹ School of Geographical Science, Qinghai Normal University, Xining 810008, China; 201947341017@stu.qhnu.edu.cn (W.M.); jiawei1212@qhnu.edu.cn (W.J.); 201947331031@stu.qhnu.edu.cn (P.S.); liufenggui@igsnr.ac.cn (F.L.)
- ² Faculty of Geographical Science, Beijing Normal University, Beijing 100875, China; 201811051120@mail.bnu.edu.cn
- ³ Academy of Plateau Science and Sustainability, Xining 810008, China
- * Correspondence: jwang@bnu.edu.cn

Abstract: In this paper, we use the extraction method of multi-factors fusion to extract the Highland barley cultivation area on Qinghai–Tibet Plateau. The study results indicate that: (1) the method (extracting through multi-factors fusion) is efficient during the extracting process and is highly accurate in extraction results. This extraction scheme allows for not only the spatial heterogeneity of different physical geographic units, but also the impact of multi-factors on crop cultivation; (2) according to our research, the total Highland barley cultivation area on Qinghai–Tibet Plateau is about 2.74×10^5 ha. Based on the statistics, we draw the first distribution map of the Highland barley cultivation area on Qinghai–Tibet Plateau, which upgrades its spatial distribution pattern from administrative unit to patch unit; (3) Highland barley in various divisions has a distinct spatial heterogeneity in elevation. On the whole, the Highland barley on the plateau is planted at an elevation of 2500–4500 m, up to 5200 m. Due to the impact of topography diversity, temperature, moisture, light, arable land and irrigation conditions, its cultivation area at the same elevation varies in different divisions.

Keywords: Highland barley; Qinghai–Tibet Plateau; cultivation area extraction; object-oriented extraction method; spatial distribution of Highland barley



Citation: Ma, W.; Jia, W.; Su, P.; Feng, X.; Liu, F.; Wang, J. Mapping Highland Barley on the Qinghai–Tibet Combing Landsat OLI Data and Object-Oriented Classification Method. *Land* **2021**, *10*, 1022. <https://doi.org/10.3390/land10101022>

Academic Editor: Le Yu

Received: 30 July 2021

Accepted: 27 September 2021

Published: 29 September 2021

Publisher's Note: MDPI stays neutral with regard to jurisdictional claims in published maps and institutional affiliations.



Copyright: © 2021 by the authors. Licensee MDPI, Basel, Switzerland. This article is an open access article distributed under the terms and conditions of the Creative Commons Attribution (CC BY) license (<https://creativecommons.org/licenses/by/4.0/>).

1. Introduction

Since the 21st century, rapid climate change has caused a severer impact of agricultural disasters, making the assessment of crop losses a research hotspot in natural disaster risk assessment [1]. Natural disaster exposure research of crops is the prerequisite for crop loss assessment. The data of crop's spatial distribution have become an urgent requirement for crop disaster loss assessment. As one of the oldest crops, barley is widely planted all over the world [2]. Highland barley, a variety of genus barley, shows strong geoherbism on Qinghai–Tibet Plateau [3] and is recognized as a predominant crop, because it adapts best to the relatively harsh natural environment of the plateau. Various ethnic groups such as the Tibetan, Qiang and Naxi who live on the plateau regard it as an essential food crop [4,5]. Due to the influence of climate change, the upper limit of elevation for Highland barley cultivation is gradually rising, and the unstable climate in the high-elevation areas leads to unpredictable cultivation [6]. Due to the limited cultivated land resources in the Qinghai–Tibet Plateau, new cultivated land is bound to be reclaimed along with the elevation of Highland barley cultivation. For the newly reclaimed Highland barley land, we also need to choose reasonable management strategies according to different land attributes. Therefore, it is urgent and necessary to understand the spatial distribution of Highland barley cultivation.

In recent years, researches on Highland barley mainly focus on three aspects: its physiological characteristics [7], nutritional value [8] and medicinal value [9]. They provide references for an in-depth study on the characteristics of Highland barley. However, the current data of its spatial distribution pattern is measured by county-level administrative unit, and it is impossible to carry out a high-accuracy quantitative assessment of natural disaster exposure of Highland barley [10]. We need to study it at a higher scale level so as to obtain a more accurate spatial distribution.

Remote sensing technology can provide stable and accurate simultaneous observation results of wide-range earth's surface. It has become an effective means for agricultural cultivation monitoring and can efficiently detect crop cultivation areas. Many satellite programs (such as Landsat, Modis, Aster, SPOT, Sentinel-1 and Sentinel-2) are nowadays providing free datasets, thus promoting satellite imagery exploitation for many agricultural applications [11]. Low-resolution and medium-resolution image data such as MODIS, Landsat TM/OLI, Sentinel-2 and GF-1 WFV have been widely used in studies of extracting rice, wheat, rapeseed and other crops [12–15]. Among them, the combination of MODIS data and vegetation index is a main approach to monitor large-scale crop [16,17]. However, with low spatial resolution and a large number of mixed pixels, MODIS data-based extraction result has a lower accuracy than the higher resolution image data [18]. As for small and medium scale crop areas, the common remote sensing image data consist of Landsat TM/OLI, Sentinel-2 and GF-1 WFV. The result of the development of unmanned aerial vehicle (UAV) technology and high-resolution MS images, the managers and specialists in agriculture can use new tools and have more information to optimize management decisions and formulate precision farming solutions [19]. In the extraction of crops, finding an appropriate way to balance the cost–benefit relationship is of great significance. Many research results show that, medium-resolution-based extracting result has a higher accuracy than the low-resolution image data.

The common methods used to extract crop distribution are supervised classification [20], artificial neural network [21], and random forest classification [22]. These above methods use spectral information of pixels, yet they overlook the texture information within the category and the interaction among the neighborhoods of the pixel [23,24]. The object-oriented classification method integrates the spectral and geometric characteristics of images, takes the segmented object as the target and analyzes the essential characteristics of the image object and the topological relationship between neighboring objects, which can effectively improve the spatial analysis ability of computer analyzing [25].

In order to obtain the high-accuracy spatial distribution of Highland barley, this paper uses Landsat 8 OLI images to extract its cultivation area through the following steps: (1) refer to China's comprehensive agricultural zoning for division; (2) limit the extent of agricultural areas with the digital elevation model (DEM) and slope data; (3) use optimum index factor (OIF) to optimize the best band for Highland barley extraction; (4) use object-oriented classification method to extract the Highland barley cultivation area on Qinghai–Tibet Plateau.

After obtaining the current spatial distribution information of Highland barley, we will also analyze the spatial distribution information of highland barley 30 years ago in the future work to analyze its dynamic changes. Since GF-1 WFV and Sentinel-2 began service in 2013 and 2016, respectively, the time series of image acquisition is relatively short. Landsat TM/OLI, which began to provide remote sensing images in 1984, has a long enough time series to meet the research needs, so we adopt Landsat 8 OLI images as the remote sensing image data [26]. We hope the final data will contribute to the quantitative analysis of Highland barley exposure and its future disaster loss assessment.

2. Study Area

The Qinghai–Tibet Plateau, known as the third pole of the earth, has an average elevation of more than 4000 m, making it the highest plateau in the world. Due to the alpine and complex natural geographical features, it has become the “initiator” and “regulatory

zone” of global climate change [27]. Located in western and southwestern China, the plateau covers an approximate total area of $2.53 \times 10^6 \text{ km}^2$ and contains vast territory and diverse landforms. It stretches over the whole area of Tibet Autonomous Region and Qinghai Province, parts of Sichuan, Yunnan, Gansu Province and Xinjiang Uygur Autonomous Region (Figure 1). Most part of the plateau belongs to arid and semi-arid areas: the northern zone is dominated by arid areas, and the central and southern zones are dominated by semi-humid and humid areas. In this region, the annual average temperature range is from $-5.75 \text{ }^\circ\text{C}$ to $2.57 \text{ }^\circ\text{C}$, the annual sunshine duration is from 2500 to 3400 h, and the annual total solar radiation is at 5000 to 8500 MJ/m^2 . It is one of the most important alpine agricultural and pastoral areas in the world [28,29]. Agricultural land is mainly distributed in valley areas below 4600 m above sea level, and most is concentrated in Hehuang Valley (in Qinghai Province) and YLN region (the region along the Yarlung Zangbo River, Lhasa River and Nianchu River in Tibet Autonomous Region). Main crops include wheat, Highland barley and rapeseed [30]. To study the impact of topographical factors and to specifically extract Highland barley, this paper refers to the Chinese agricultural division scheme proposed by Zhou Lisan [31] and divides the plateau into seven major agricultural divisions, which is mainly based on natural conditions, agricultural production status and social economy conditions. The seven major agricultural divisions are as follows, I: Inner Mongolia, Gansu and Ningxia farming–pastoral division (IMGN/FPD), II: Central Gansu and Eastern Qinghai farming–pastoral division (CGEQ/HFD), III: Qinghai and Gansu farming–pastoral division (QG/FPD), IV: South Xinjiang farming–pastoral division (SX/FPD), V: Qinghai–Tibet alpine pasturing division (QT/APD), VI: South Tibet farming–pastoral division (ST/FPD), VII: Sichuan–Tibet forest and farming–pastoral division (ST/FFD).

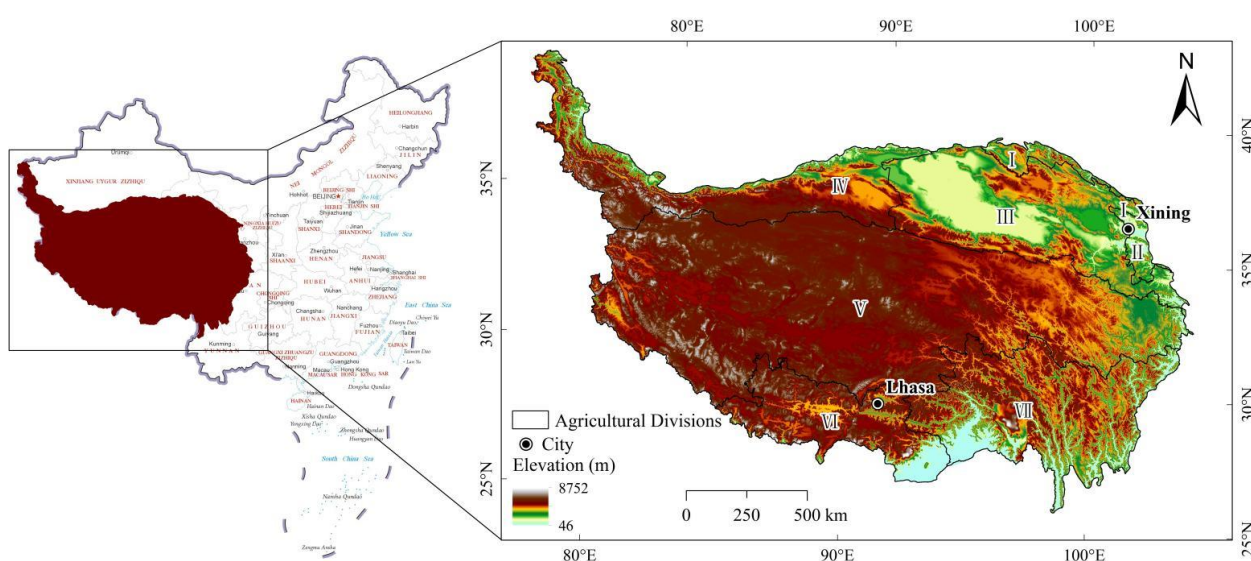


Figure 1. Agricultural divisions on the Qinghai–Tibet Plateau.

3. Materials and Methods

3.1. Data Collection

We adopt Landsat 8 OLI images as the remote sensing image data (Table 1). The data are based on summer images and the imaging time is mainly from June 2019 to September 2019, select images with less than 10% cloud cover. Due to the extensive study area, in some parts on the southern plateau, large amount of water vapor causes cloud cover, which blocks out the earth surface. The 2019 summer images in these areas could not meet the requirements, and they were replaced by the summer images from the nearest year. We have a total number of 96 scenes in this paper.

Table 1. Landsat 8 OLI sensor parameter.

Band	Wavelength Range	Spatial Resolution	General Purpose
1-COASTAL/AEROSOL	0.43–0.45 μm	30 m	Coastal environmental monitoring
2-Blue	0.45–0.51 μm	30 m	Visible light three-band True color is used for feature recognition
3-Green	0.53–0.59 μm	30 m	
4-Red	0.64–0.67 μm	30 m	
5-NIR	0.85–0.88 μm	30 m	
6-SWIR1	1.57–1.65 μm	30 m	Vegetation information extraction Vegetation drought monitoring Fire monitoring
7-SWIR2	2.11–2.29 μm	30 m	Mineral information extraction
8-PAN	0.50–0.68 μm	15 m	Feature recognition Data fusion
9-Cirrus	1.36–1.38 μm	30 m	Cirrus detection Data quality evaluation

The boundary data of Qinghai–Tibet Plateau used in this paper are the vector data released by Zhang Yili from the Global Change Scientific Research Data Publishing System [32]. This paper uses the Qinghai–Tibet Plateau DEM data with a spatial resolution of 30 m (Table 2).

Table 2. Statistics of Highland barley planting areas in various agricultural divisions.

Data Name	Temporal Resolution	Spatial Resolution	Data Source
Landsat 8 OLI images	2019	30 m \times 30 m	Institute of Geographic Sciences and Natural Resources Research, CAS http://ids.ceode.ac.cn (accessed on 30 September 2020) [33]
Digital elevation model	2010	30 m \times 30 m	United States Geological Survey https://topotools.cr.usgs.gov (accessed on 15 March 2020)
Multi-year average precipitation	1961–2019	-	China Meteorological Data Network http://data.cma.cn (accessed on 1 January 2020)
Map of China	2019	-	Ministry of Natural Resources of the People’s Republic of China http://bzdt.ch.mnr.gov.cn (accessed on 25 August 2021)
Qinghai–Tibet Plateau range and boundary line	2014	-	Global Change Research Data Publishing & Repository http://www.geodoi.ac.cn (accessed on 1 January 2020)

3.2. Remote Sensing Image Preprocessing

The remote sensing image data are preprocessed by ENVI 5.3 and ArcGIS 10.3. The steps are as follows: (1) Use the three parameters of spectral radiance value of each band, solar elevation angle and shooting time for Radiometric Calibration. Set the Calibration Type to Radiance; set the Data Type to Float; set the Scale Factor to 0.1; (2) Use FLAASH model for atmospheric correction. Atmospheric models are selected based on water vapor data or surface air temperature, fill in the Ground Elevation, Flight Date and Flight Time, select Aerosol Retrieval as 2-Band (K-T); set Water Retrieval to NO; (3) take the Gram-Schmidt method to convert panchromatic B8 (15 m) fusion with the multispectral band (30 m), and increase the spatial resolution of the multispectral band to 15 m. The result of the fusion is shown in Figure 2.

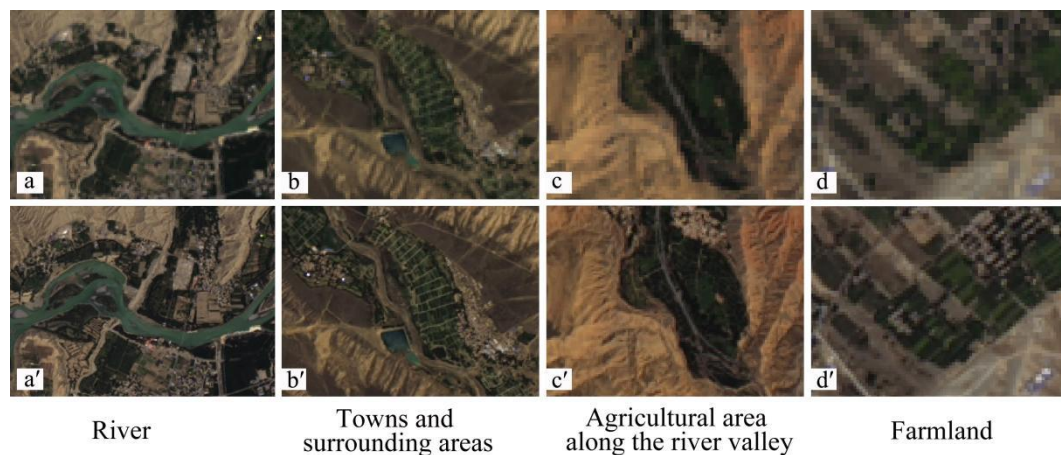


Figure 2. Comparison before and after OLI image fusion. (a–d) show the image before fusion, and (a'–d') are after fusion.

After fusion, we cut the vector boundary of the study area to generate the work base image map, and obtain the slope data of the plateau from the DEM data.

3.3. Sample-Based and Object-Oriented Information Extraction Methods

The object-oriented sample information-based extraction method takes the object generated by segmenting the entire image as the research target, and the size of the object is determined by the image segmentation scale and spatial structure. When extracting information, not only the spectral feature difference of the image is considered, but also spatial features such as the texture and shape of the features in the image and the relationship structure information among various objects are considered [34]. The object-oriented sample information-based extraction method encompasses two main steps: (1) the “segmentation”, which is the delineation of homogeneous objects from the input imagery, following the principle of clustering neighboring image pixels into “objects”, so as to maximize the intra-object spectral homogeneity and inter-object spectral heterogeneity; (2) the “classification”, which labels and assigns each polygon to the target cover class [35].

OLI image shows an enhancement in spectral heterogeneity after band fusion. And its pixels contain more information, such as structural features, texture information, and the interconnection with neighboring features. Using the multi-scale segmentation algorithm could fully take advantage of these abundant information. Multi-scale segmentation is an object-oriented image segmentation algorithm. It can segment an image into “homogeneous” objects, and the object size is determined by the segmentation scale. Any object after segmentation has the same or very similar features, such as spectrum and shape, and each object interacts with each other, but not overlaps. We use it to segment the remote sensing images at the optimal scale, and then merge images according to geometric and spectral differences of the pixel objects.

The setting of segmentation parameters is the most important part of the whole multi-scale image segmentation process. The steps are as follows: (1) an appropriate scale threshold is set to terminate pixel merging; (2) according to the spectral information, texture characteristics and characteristics of the ground object type to be extracted, appropriate weights are given to the spectrum and shape factors. The shape factor includes compactness and smoothness, which are determined by the structural characteristics of the ground objects to be extracted from the image; (3) the image segmentation starts with any pixel in the image as the center. The segmentation process is completed when it exceeds the given threshold. We repeat experiments until the results match the terrain information in the images. In each agricultural division, we set the segmentation threshold at 20–30, and the merging threshold at 80–90. The results are shown in Figure 3. All these parameters were empirically found to ensure the best results for delineation of desired segmentation, using the trial and error approach.

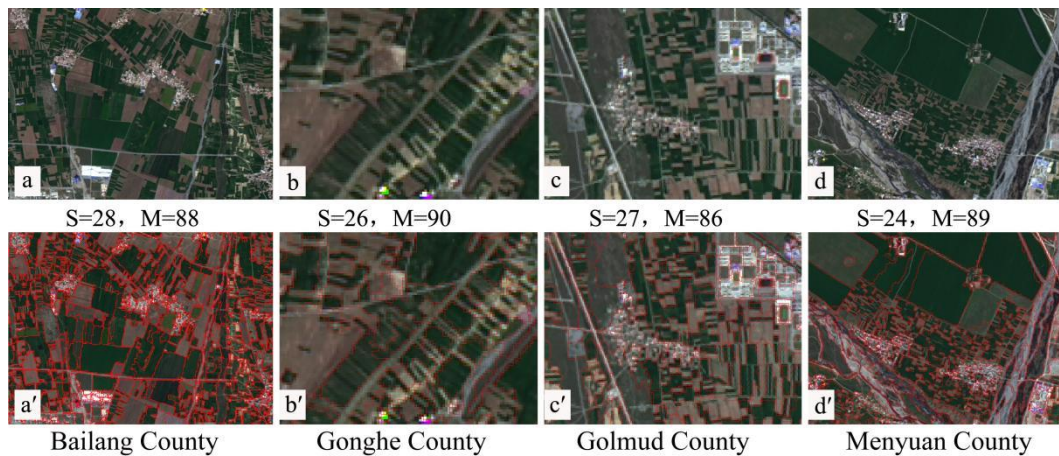


Figure 3. Segmentation results under different segmentation scales. (a–d) show the image before segmentation, and (a'–d') are after segmentation.

3.4. Band Optimization

OLI image consists of seven multi-spectral bands, which contain detailed feature information. This paper uses the optimal waveband method to obtain the optimal band for Highland barley extraction in each agricultural division, in order to reduce the data redundancy. We select the Optimal band through the optimal index factor (OIF) (Equation (1)) [36], which is based on the interrelationship of the information quantity of image bands. It integrates the standard deviation of a single band and the correlation between bands. The higher value of OIF presents richer combined information quantity and lower redundancy, thus providing a better solution. We select the bands with richer information quantity, lower correlation, distinct spectral differences and higher differentiation index as the best solution. The formula of calculating OIF is shown as follows:

$$\text{OIF} = \frac{\sum_{i=1}^n S_i}{\sum_{j=1}^n |R_{ij}|} \quad (1)$$

where n is the number of image bands, S_i is the standard deviation of the reflectance value of i -th band, and $|R_{ij}|$ is the absolute value of the correlation coefficient of two bands.

3.5. Highland Barley Cultivation Extent Restriction

The terrain of Qinghai–Tibet Plateau slopes from northwest to southeast, representing a strong regional differentiation. Among the seven divisions, there are five Highland-barley divisions (consisting of ST/FPD, ST/FFD, QG/FPD, QT/APD and CGEQ/HFD), and two non-Highland-barley planting divisions (MGN/FPD and SX/FPD).

We judge the agricultural land through elevation and slope factors based on the topography of each division. A Chinese reforestation policy requires that the cultivated land steeper than 30° should be converted into woodland, because it is not suitable for planting crops [37]. Therefore, the upper limit of the slopes for growing Highland barley is 30° . The highest cultivation elevation is different in each division, shown as follows: 3600 m in CGEQ/HFD; 4500 m in QG/FPD; 5000 m in QT/APD; 5500 m in ST/FPD; 5200 m in ST/FFD. Then we turn to the influence of precipitation. The multi-year average precipitation on the plateau is about 470 mm. There has a significant distribution variability of rainfall on the plateau: it is the most abundant in the southeastern plateau, and least abundant in Qaidam Basin and Qiangtang Plateau (in the north and west of the Qinghai–Tibet Plateau), where the rainfall cannot meet the needs for Highland barley cultivation. In this study, we remove areas with an annual precipitation less than 250 mm, unless they provide irrigation conditions that can satisfy the growing needs of Highland barley. Agricultural areas with satisfactory irrigation conditions consist of the oasis agricultural areas in Golmud, Dulan, Ulan and certain places in Qaidam Basin [38].

3.6. Accuracy Verification

This paper uses the Confusion Matrix to verify the accuracy of the extraction results [39]. We select QG/FPD as the typical area for field sampling in June 2020. We selected 109 highland barley sample points and 109 other crop sample points. The major sampling process is to obtain the latitude and longitude of each sample point through high-precision handheld GPS units, measure its slope by Clinometer, take photographs of the landscape nearby for the subsequent verification. The distribution of sample points is shown in Figure 4.

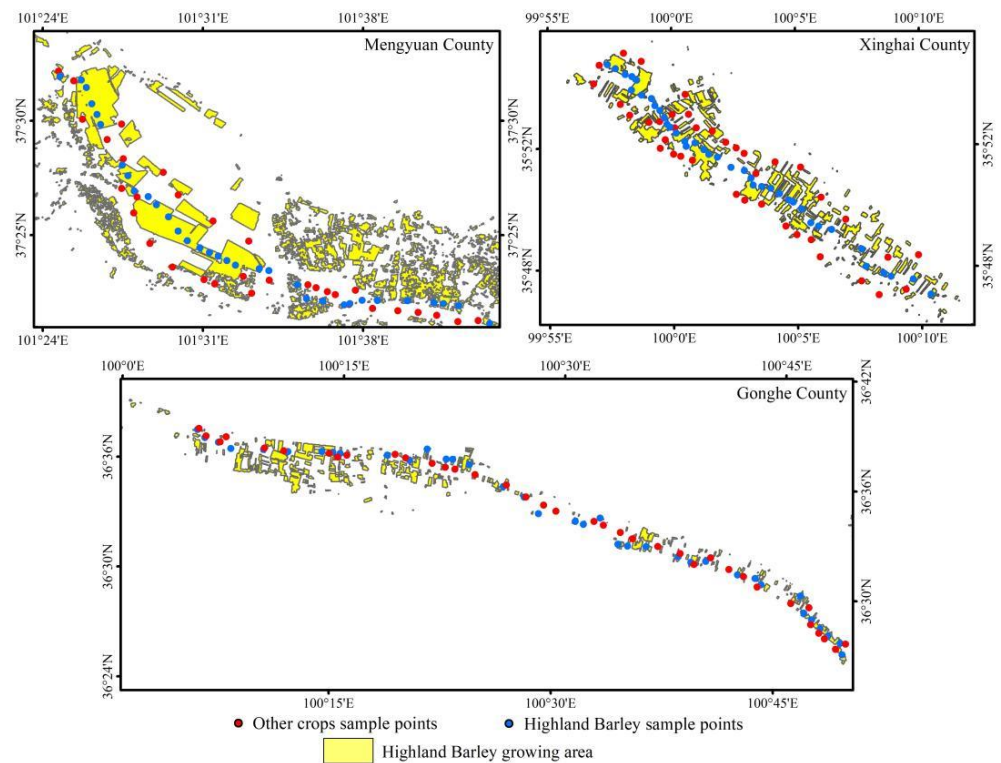


Figure 4. The location of the sample points in QG/FPD.

3.7. The Extraction Process of Highland Barley

As shown in Figure 5, this paper adopts the method of zoning, classification and multi-element fusion to efficiently perform the high-accuracy extraction.

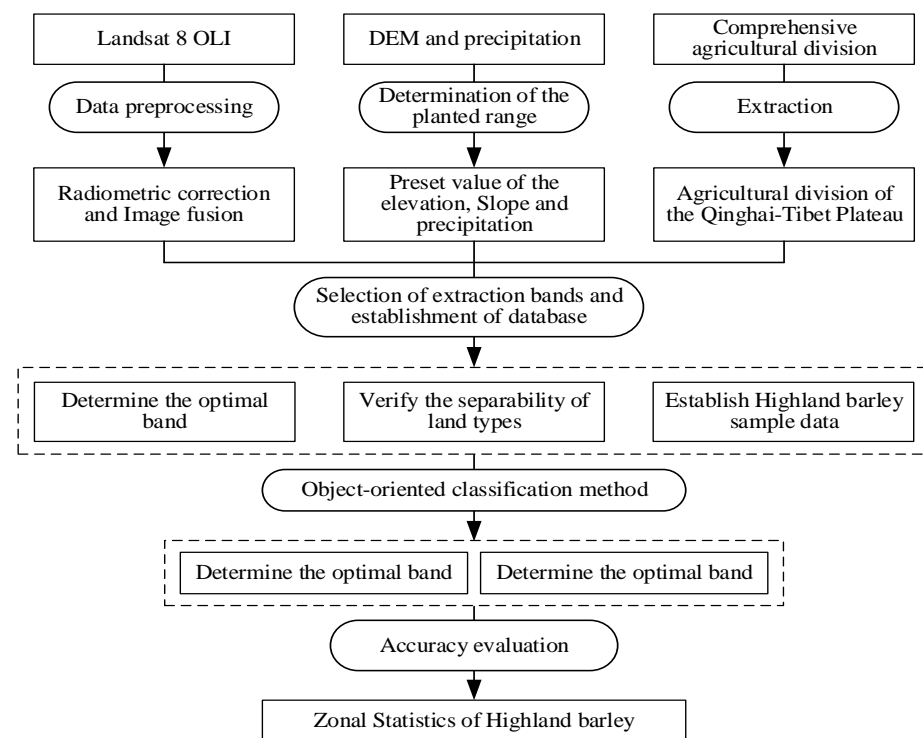


Figure 5. The extraction process of Highland barley in the Qinghai–Tibet Plateau.

4. Results

4.1. Highland Barley Extraction Based on Sample Information

Under the optimal segmentation scale, the cultivation area of Highland barley has a distinct boundary. Based on the spectral information, geometric and texture characteristics of Highland barley cultivation areas and non-Highland barley cultivation areas in each division, we construct the Highland barley sample databases for each division. These databases collect spatial and attribute information of the Highland barley, which we use to establish a sample dataset of extracted characteristic parameters. Combining the dataset with the previous field survey results, we use the support vector machine method to classify the agricultural divisions, then obtain the sample quantity taken from Highland barley in different divisions. In divisions with large patches of Highland barley (QG/FPD), the HB sample quantity at the county level is between 300 and 500, and the non-HB sample quantity is between 600 and 800; in divisions with small and continuously distributed patches of Highland barley (ST/FPD and CGEQ/HFD), the HB sample quantity is between 500 and 700, and the non-Highland barley sample quantity is about 1000; in divisions with small and evenly distributed patches of Highland barley (ST/FFD), the HB sample quantity is between 600 and 1000, and the non-HB sample quantity is about 1000; in divisions with irregularly distributed patches (QT/APD), the county-level sample quantity of HB and non-HB is adjusted according to the case (Appendix A).

4.2. Optimizing the Bands of Highland Barley Extraction in Each Agriculture Area

According to the calculation, the optimal extraction bands for CGEQ/HFD and ST/FPD are B4, B5 and B7; for QG/FPD and QT/APD are B1, B4 and B5; for ST/FFD are B1, B5 and B6. Next, we verify whether rapeseed might affect the extraction of Highland barley after band optimization treatment. To this end, we randomly select 100 typical samples each of Highland barley and rapeseed from each agricultural division, and draw the optimal band spectral characteristic curve (Figure 6). The results show that, in each agricultural division, Highland barley has a distinct difference with other major crops in reflectance spectra after the optimal wavebands, revealing a fine discrimination index.

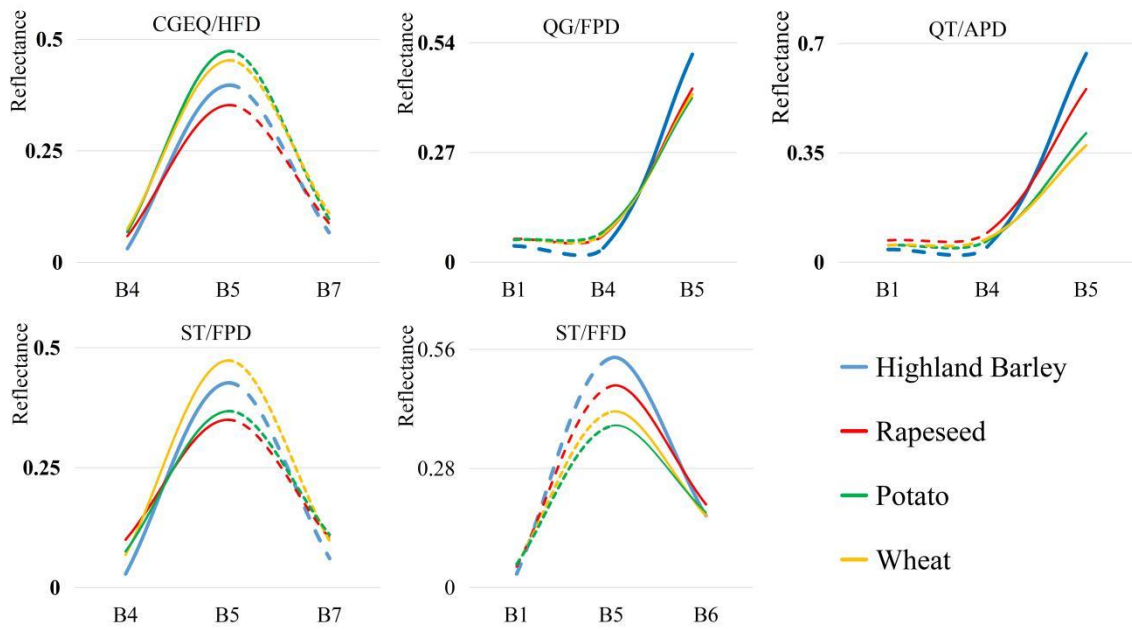


Figure 6. Surface reflectance curves of Highland barley and rapeseed in various agricultural divisions.

4.3. The Extraction Results of Highland Barley

The extraction results indicate that the total cultivation area of Highland barley on the plateau is 2.74×10^5 ha, and it mainly grows in the eastern and southern plateau (Figure 7). We sort the 5 agricultural divisions from the largest to the smallest in terms of Highland barley cultivation area: QG/FPD, ST/FPD, ST/FFD, QT/APD, and CGEQ/HFD, accounting for 31.09%, 28.91%, 23.23%, 11.86% and 4.91%, respectively, of the total area of each division.

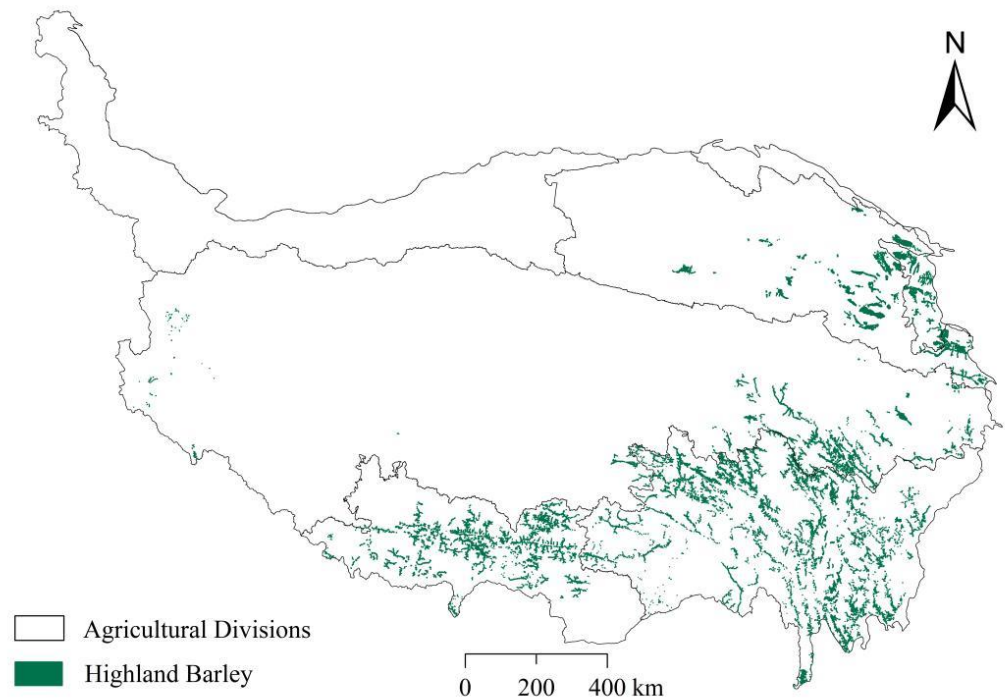


Figure 7. The extraction results of Highland barley on the Qinghai-Tibet Plateau.

4.4. Results of Accuracy Verification

The confusion matrix was used to evaluate the accuracy of Highland barley extraction results. Table 3 shows that the accuracy of extraction results is relatively good, with Kappa coefficient up to 0.83 and Producer's Accuracy and User's Accuracy both over 90%.

Table 3. Evaluation of the accuracy of Highland barley extraction results.

Type	Producer's Accuracy (Pixels)	User's Accuracy (Pixels)	Producer's Accuracy (%)	User's Accuracy (%)	Overall Accuracy (%)	Kappa Coefficient
Highland barley	99/109	99/107	90.83	92.52	91.74	0.83
Other crops	101/109	101/111	92.66	90.99		

5. Discussion

5.1. Classification and Statistics of Highland Barley Cultivation Area

We count the Highland barley cultivation area in five agricultural divisions at different elevation ranges, as shown in Table 4. We divide it into eight ranges at 500 m intervals. In general, 5200 m is the current upper limit of elevation for growing Highland barley, and the elevation range of 2500–4500 m concentrates the most patches, which accounts for 94.43% of the total Highland barley planting area on the plateau. Within the elevation range lower than 2500 m, its cultivation land accounts for 4.84%. By contrast, the elevation range above 4500 m only accounts for 0.73%.

Table 4. Statistics of Highland barley planting areas in various agricultural divisions.

Agricultural Divisions	CGEQ/HFD	ST/FPD	ST/FFD	QT/APD	IMGN/FPD
Proportion of Highland barley planting areas	31.09%	28.91%	23.23%	11.86%	4.91%
Proportion of Highland barley planting areas in different elevation ranges					
<2000 m	0.29%	0.00%	1.72%	0.08%	2.20%
2000 to 2500 m	2.24%	0.00%	6.82%	0.73%	37.33%
2500 to 3000 m	32.05%	0.14%	14.42%	3.86%	52.84%
3000 to 3500 m	65.40%	0.46%	20.29%	22.19%	7.62%
3500 to 4000 m	0.02%	46.51%	32.99%	45.74%	0.00%
4000 to 4500 m	0.00%	50.68%	23.45%	27.13%	0.00%
4500 to 5000 m	0.00%	2.16%	0.32%	0.27%	0.00%
≥5000 m	0.00%	0.05%	0.00%	0.00%	0.00%
Proportion of Highland barley planting area in different slope ranges					
<5°	87.97%	76.28%	18.24%	40.14%	66.06%
5 to 10°	6.69%	14.53%	19.70%	18.94%	21.95%
10 to 15°	2.38%	5.21%	16.19%	13.44%	8.10%
15 to 20°	1.08%	2.08%	13.35%	9.66%	1.99%
≥20°	1.87%	1.91%	32.53%	17.82%	1.90%

We divide the slope gradient of each division into 5 ranges, including <5°, 5°–10°, 10°–15°, 15°–20°, ≥20°, and count the cultivation area at each slope range in 5 agricultural divisions. Overall, in QG/FPD, ST/FPD and CGEQ/HFD, most Highland barley patches are at the slope of <5°, accounting for 87.97%, 76.28% and 66.06% of each division's total agricultural area, respectively. In these three divisions, only a small proportion of HB patches is at a slope of ≥20°, accounting for 1.87%, 1.91% and 1.90%, respectively. In QT/APD, most HB patches are at a slope of <5°, accounting for 40.13%; that at a slope of ≥20° accounts for 17.82%, and the least are at the slope range of 15°–20°, accounting for 9.66%. In ST/FFD, the HB patches at the slope range of <5°, 5°–10°, 10°–15°, 15°–20° accounts for 18.24%, 19.70%, 16.19% and 13.35%, respectively, showing an even distribution at the slope below 20°; the slope range of ≥20° has the largest amount of cultivation areas, accounting for 32.52%. These distribution characteristics might be related to the fragmentation degree of the land patch in this division.

5.2. The Relationship between Highland Barley and Elevation

Due to strong spatial heterogeneity, each of the divisions has clearly different distribution patterns of Highland barley, as shown in Figure 8. QG/FPD has the largest Highland barley cultivation area, and 65.40% of them occurs at the elevation of 3000–3500 m. In QG/FPD, most of the Highland barley is continuously distributed in river valleys, mountain basins and flat slopes along the plateau surface (Figure 8e). In Qaidam Basin, Highland barley cultivation areas are found in the oasis agricultural zone (Figure 8c). In ST/FPD, Highland barley is mostly planted in Yarlung Zangbo River Valley (Figure 8g) where there has fine hydrothermal condition and continuous and flat land. In this division, most HB patches are at the range of 3500–4500 m, up to 5000 m or higher, making it the only area that can have Highland barley grown above 5000 m a.s.l. on the plateau, though most of these patches are small and scattered along the valley (Figure 8f). In ST/FFD and QT/APD, the HB patches are at the range of 3000–4500 m a.s.l., most in fragmented patches along the river valleys (Figure 8a,d,h); CGEQ/HFD is the area at the lowest elevation and has the smallest barley cultivation area on the plateau. In this division, Highland barley is mainly distributed at the range of 2000–3000 m a.s.l., and mostly in fragmented patches of the valley at high elevation (Figure 8b).

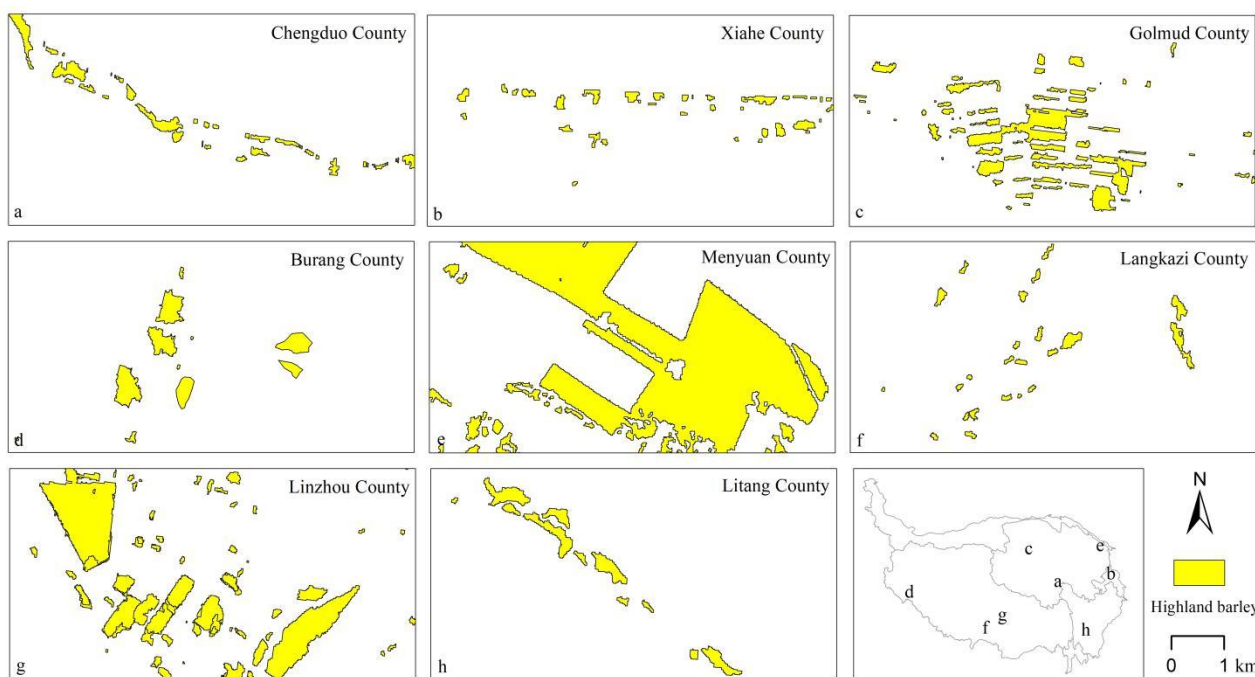


Figure 8. Distribution patterns of Highland barley under different elevation and different hydrological elements.

The above results indicate that Highland barley cultivation areas show various distribution characteristics at different elevation ranges, because each division varies in the terrain, temperature, moisture, light, distribution range of arable land, and irrigation conditions. For example, the elevation of 3500 m is the upper limit in CGEQ/HFD, while in ST/FPD, the area at the elevation above 3500 m concentrates most of the HB cultivation areas (Figure 9).

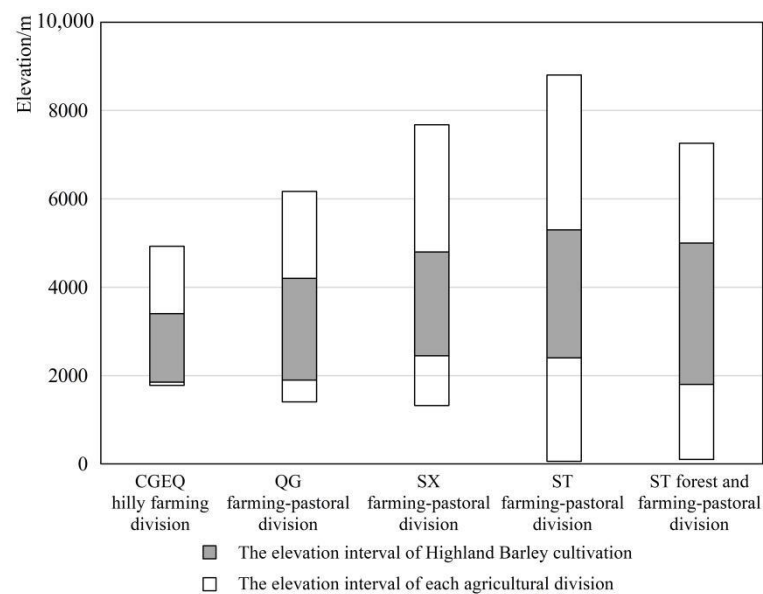


Figure 9. The elevation interval of Highland barley cultivation and each agricultural division.

5.3. Ways to Improve the Accuracy of Remote Sensing Extraction of Highland Barley Area

The accuracy of Highland barley extraction results is limited by three factors: the fragmentation degree of each division, the asynchrony of the growing period of Highland barley in each division, and the similarity between other crops and Highland barley in spectral characteristics. We could improve the accuracy of Highland barley extraction in further studies in following aspects. First, improve the spatial resolution of remote sensing images [40]. At the present stage, using the spatial resolution of 15 m is difficult to identify Highland barley in certain regions due to various fragmentation degrees. Second, optimize the temporal resolution of Highland barley extraction. The broad span causes various growth period of Highland barley in each division. It would be better to count the growing period of the Highland barley in each division, and select the barley-extraction optimal period when its spectral characteristics are distinct from other crops. Third, optimize the extraction results by restricting suitable conditions for Highland barley [41]. In this paper, we restrict the Highland barley distribution from the aspects of elevation and slope, and further studies can discuss accumulated temperature, sunshine duration, etc.

6. Conclusions

This paper uses OIF images, selects the best bands extracted from Highland barley, and takes the object-oriented classification method to extract the Highland barley cultivation area on Qinghai–Tibet Plateau. Based on the above analysis, we draw the following conclusions:

We propose a multi-factor fusion based on sub-region classification method for efficiently extracting Highland barley images. Depending on the agricultural divisions, we use multiple factors (including elevation, slope, rainfall and hydrology) to restrict the extent of Highland barley's pattern spots; we use image segmentation technology to build division-based Highland barley extraction samples; we use Gauss radial basis kernel in support vector machines (SVMs) to obtain the extraction results with superior accuracy.

According to the extraction results, the total Highland barley cultivation area of 5 divisions is about 2.74×10^5 ha. We draw the first distribution map of Highland barley cultivation area on Qinghai–Tibet Plateau based on the data. The map shows that the largest amount of Highland barley is grown in the eastern and southern plateau. Through the map, we could learn the spatial distribution pattern of Highland barley from the patch scale (previously from the administrative unit scale). On this basis, we could conduct in-depth studies on the distribution of HB suitable areas under different scenarios, which might optimize the Highland barley's spatial distribution and provide reference indicators for the quantitative assessment of its disaster exposure. At the same time, it can provide data

references for other researches about Qinghai–Tibet Plateau, such as future development of characteristic agriculture, security of state grain reserves and decision-making in response to climate change.

The distribution of Highland barley cultivation land shows a distinct spatial heterogeneity in different elevation ranges. Overall, Highland barley is distributed in the range of 2500–4500 m, up to 5200 m. When at the same elevation, the factors that affect Highland barley’s growing (such as topography, temperature, moisture, light, distribution of arable land and irrigation conditions) vary in each division, and therefore the cultivation scale is different to each other. At the same elevation, the Highland barley in CGEQ/HFD is planted on the fragmented and steep sloping lands that have the farthest distance from the river, while in ST/FPD, it is planted on the continuous and flat lands in the center of river valleys.

Author Contributions: W.M. conducted the research, analyzed the data and wrote the paper; W.J. processed the data; F.L. guided the research and extensively updated the manuscript; J.W. conceived the research and provided project support; P.S. and X.F. helped process the data. All authors have read and agreed to the published version of the manuscript.

Funding: This research was funded by the Second Qinghai–Tibet Plateau Scientific Expedition and Research Program (STEP), grant number 2019QZKK0606 and the National Key Research and Development Program of China, grant number 2016YFA0602402.

Data Availability Statement: All data and materials are available upon request.

Acknowledgments: We are particularly indebted to Peijun Shi and Xingsheng Xia from the Qinghai Normal University for their constructive suggestions on an earlier draft of this paper.

Conflicts of Interest: The authors declare no conflict of interest.

Appendix A. Highland Barley Extraction Area of Counties in Different Divisions

Table A1. CGEQ/HFD.

County	Area (ha)	County	Area (ha)	County	Area (ha)
Datong	1379.34	Ledu	812.67	Huzhu	3496.05
Hualong	4564.58	Tongren	1200.35	Xiahe	1258.40
Jianzha	380.07	Xunhua	389.99		

Table A2. QT/APD.

County	Area (ha)	County	Area (ha)	County	Area (ha)
Aba	4722.81	Pulan	498.01	Maerkang	642.17
Baqing	34.34	Rangtang	1079.89	Nima	31.72
Biru	1566.59	Ritu	173.12	Heishui	609.99
Gaier	133.97	Zoige	762.80	Jiali	199.64
Geji	12.83	Saga	225.09	Zhada	212.88
Yushu	2489.11	Songpan	583.56		

Table A3. QG/FPD.

County	Area (ha)	County	Area (ha)	County	Area (ha)
Delingha	1143.29	Huangzhong	1181.14	Haiyan	938.81
Diebu	1151.98	Lintan	1296.00	Hezuo	2760.95
Dulan	8187.53	Luqu	1046.70	Huangyuan	622.89
Gangcha	100.00	Menyuan	11,297.36	Zeku	1084.57
Golmud	1196.64	Qilian	1085.78	Zhouqu	1434.17
Gonghe	14,105.70	Tongde	5754.35	Zhuoni	861.86
Guide	626.45	Wulan	753.25		
Guinan	17,148.20	Xinghai	5406.80		

Table A4. ST/FFD.

County	Area (ha)	County	Area (ha)	County	Area (ha)
Basu	1578.10	Gongbujiangda	2032.27	Luolong	3051.00
Batang	1340.96	Gongjue	2706.73	Muli	1161.31
Bayi	240.93	Gongshan	229.10	Seda	721.10
Baiyu	3040.79	Jiacha	995.60	Suo	1433.10
Bianba	3088.20	Jiangda	4119.39	Weixi	1205.71
Bomi	1445.40	Jiulong	143.24	Xiangcheng	878.09
Chaya	2920.20	Karuo	4125.24	Xianggelila	3660.54
Chayu	892.10	Kangding	2119.79	Xinlong	2324.57
Danba	257.11	Lanping	237.42	Yajiang	1544.52
Daofu	2843.57	Langxia	594.45	Mangkang	2151.20
Daocheng	1835.31	Leiwuqi	2838.30	Milin	785.30
Derong	720.70	Litang	2569.01	Motuo	94.50
Deqin	791.55	Luhuo	2890.85	Yulong	919.35
Dingqing	6123.15	Lushui	532.73	Zuogong	1976.40

Table A5. ST/FPD.

County	Area (ha)	County	Area (ha)	County	Area (ha)
Angren	3988.97	Jilong	672.89	Nimu	1325.03
Bailang	5316.98	Jiangzi	6008.92	Nielamu	1275.54
Banma	246.60	Kangma	2112.89	Qiongjie	893.18
Chengguan	266.38	Lazi	4372.94	Qushui	1699.76
Cuomei	662.16	Langkazi	1575.53	Qusong	800.33
Cuona	915.95	Linzhou	5714.82	Renbu	1157.63
Dazi	1357.72	Longzi	1458.27	Sajia	4146.10
Dingjie	2136.42	Maqin	435.15	Sangri	361.28
Dingri	6427.01	Mozhugongka	2373.86	Sangzhuzi	6069.92
Duilogdeqing	2637.92	Naidong	941.37	Xietongmen	1641.20
Gangba	790.47	Nanmulin	4322.75	Yadong	194.78
Gongga	2296.08	Nangqian	2432.18	Zhanang	1868.76

References

- Wang, R.; Jiang, Y.; Zhang, A.; Gao, Y.; Wang, J. Review on crop exposure of natural disasters. *J. Catastr.* **2019**, *34*, 215–221. [\[CrossRef\]](#)
- Xu, M. Study on World Barley Trade Pattern and Its Influence on Chinese Barley Industry. Ph.D. Thesis, Chinese Academy of Agricultural Sciences, Beijing, China, 2013.
- Meng, J.; Li, H.; Zhang, Q.; Li, M.; Liu, S. Effect of growth conditions on the Yield and nutrient quality of Hulless Barley. *J. Anhui Agric. Sci.* **2017**, *45*, 30–38. [\[CrossRef\]](#)
- Yin, Z.; Ouyang, H.; Zhang, X. Study on water consumption of Spring Naked Barley Land and suitable irrigation system in Tibet. *J. Nat. Resour.* **2010**, *25*, 1666–1675. [\[CrossRef\]](#)
- Fan, Y.Z.; Zhong, Z.M.; Zhang, X.Z. A comparative analysis of photosynthetic characteristics of hulless barley at two altitudes on the Tibetan Plateau. *Photosynthetica* **2011**, *49*, 112–118. [\[CrossRef\]](#)
- Basang, Y.; Liu, X.; Fu, G.; Li, D. Genetic diversity and population structure analysis of hulless barley with Cold Tolerance from the Qinghai-Tibetan Plateau Revealed by SSR Markers. *J. Triticeae Crops* **2017**, *37*, 40–47. [\[CrossRef\]](#)
- Qi, Y.; Cao, S.; Li, X.; Li, M. Fusarium avenaceum infection: Effects on physiological indexes of leaves and roots of naked barley with different resistance. *Chin. Agric. Sci. Bull.* **2019**, *32*, 101–107.
- Zhu, F.; Du, B.; Xu, B. Superfine grinding improves functional properties and antioxidant capacities of bran dietary fibre from Qingke (hull-less barley) grown in Qinghai-Tibet Plateau, China. *J. Cereal Sci.* **2015**, *65*, 43–47. [\[CrossRef\]](#)
- Hu, H.; Liu, P.; Cheng, P.; Wang, W.; Liu, Y. Study on the Auxiliary Hypoglycemic function of small molecule β -Glucan from Hull-less Barley. *Food Res. Dev.* **2018**, *39*, 33–37. [\[CrossRef\]](#)
- Ma, W.; Su, P.; Jia, W.; Liu, F.; Wang, J. Advances in the research on the exposure of Highland Barley natural disasters on the background of climate change. *J. Catastr.* **2020**, *35*, 215–221. [\[CrossRef\]](#)
- Mariana, B.; Ovidiu, C. Sentinel-2 cropland mapping using pixel-based and object-based timeweighted dynamic time warping analysis. *Remote Sens. Environ.* **2018**, *204*, 509–523.

12. Boschetti, M.; Busetto, L.; Manfron, G.; Laborte, A.; Asilo, S.; Pazhanivelan, S.; Nelson, A. PhenoRice: A method for automatic extraction of spatio-temporal information on rice crops using satellite data time series. *Remote Sens. Environ.* **2017**, *194*, 347–365. [[CrossRef](#)]
13. Hui, Y.; Su, R.; Xi, W. Extraction of rape planting distribution information in Jiangnan Plain based on MODIS EVI time series data. *Remote Sens. Land Resour.* **2018**, *30*, 173–179. [[CrossRef](#)]
14. Qiu, B.; Lu, D.; Tang, Z.; Chen, C.; Zou, F. Automatic and adaptive paddy rice mapping using Landsat images: Case study in Songnen Plain in Northeast China. *Sci. Total Environ.* **2017**, *598*, 581–592. [[CrossRef](#)]
15. Zhou, Q.; Yu, Q.; Liu, J.; Wu, W.; Tang, H. Perspective of Chinese GF-1 high-resolution satellite data in agricultural remote sensing monitoring. *J. Integr. Agric.* **2017**, *16*, 242–251. [[CrossRef](#)]
16. Tao, J.; Wu, W.; Zhou, Y.; Wang, Y.; Jiang, Y. Mapping winter wheat using phenological feature of peak before winter on the North China Plain based on time-series MODIS data. *J. Integr. Agric.* **2017**, *16*, 348–359. [[CrossRef](#)]
17. Chemin, Y.; Phuphak, S.; Asilo, S. Determining spatial and temporal patterns of submergence in rice with MODIS satellite data. *Int. J. Geoinform.* **2012**, *8*, 1–12.
18. Liu, W.; Zeng, Y.; Zhang, M. Mapping rice paddy distribution by using time series HJ blend data and phenological parameters. *J. Remote Sens.* **2018**, *22*, 381–391. [[CrossRef](#)]
19. Gaetano, M.; Jose, M.P.; Marco, V.; Giuseppe, M. A Comparison of UAV and satellites multispectral imagery in monitoring onion crop. An application in the ‘Cipolla Rossa di Tropea’ (Italy). *Remote Sens.* **2020**, *12*, 3424.
20. Luo, H.; Li, W.; Jing, Y.; Xu, X.; Chen, H. Remote Sensing Extraction of Winter Wheat Planting Area Based on SVM. *J. Triticeae Crops* **2019**, *39*, 455–462. [[CrossRef](#)]
21. Liu, W.; Tao, J.; Xu, M.; Chen, R.; Guo, Y. A study of winter rape extraction at sub-pixel fusing multi-source data based on Artificial Neural Networks: A case study of Jiangnan and Dongting Lake Plain. *J. Nat. Resour.* **2019**, *34*, 1079–1092. [[CrossRef](#)]
22. Tan, S.; Wu, B.; Zhang, X. Mapping paddy rice in the Hainan Province using both Google Earth engine and remote sensing images. *J. Geo-Inf. Sci.* **2019**, *21*, 937–947. [[CrossRef](#)]
23. Ji, Z.; Zhang, Y.; Li, Q.; Liu, S.; Li, S.; Ren, H. planting information extraction of winter wheat and rape based on GF-1 images. *Remote Sens. Tech. Appl.* **2017**, *32*, 760–765. [[CrossRef](#)]
24. Quan, J.; Wang, Y.; Wang, X.; Tang, W.; Wang, Q. Extraction of Rice Planting Area in Dabie Mountain by Remote Sensing Image: Taking Landsat 8 as an example. *Chin. Agric. Sci. Bull.* **2019**, *35*, 104–111.
25. Jia, W.; Gao, X.; Yang, L.; Shi, F.; He, L. Land cover information extraction for complicated terrain regions via an object-oriented classification method. *J. Lanzhou Univ. Nat. Sci.* **2018**, *54*, 486–493. [[CrossRef](#)]
26. Aleem, K.; Lorenzo, C.; Biglia, A.; Davide, R.A.; Marcello, C.; Paolo, G. Comparison of Satellite and UAV-based multispectral imagery for vineyard variability assessment. *Remote Sens.* **2019**, *11*, 436.
27. Shi, P.; Chen, Y.; Zhang, A.; He, Y.; Gao, M.; Yang, J.; Mao, R.; Wu, J.; Ye, T.; Xiao, C. Factors contribution to oxygen concentration in Qinghai-Tibetan Plateau. *Chin. Sci. Bull.* **2018**, *64*, 715–724. [[CrossRef](#)]
28. Xu, J.; Gao, Y.; Peng, F.; Wang, X. Change characteristics of precipitation and its cause during 1979–2016 over the Qinghai-Tibetan Plateau. *Plateau Meteor.* **2020**, *39*, 234–244. [[CrossRef](#)]
29. Zhao, Y.; Wang, Y.; Xu, X.; Dong, L. Effect of the Asian Water Tower over the Qinghai-Tibet Plateau and the characteristics of atmospheric water circulation. *Chin. Sci. Bull.* **2019**, *64*, 2830–2841. [[CrossRef](#)]
30. Wei, H.; Lv, C.; Liu, Y.; Yang, K. Spatial distribution and temporal changes of facility agriculture on the Tibetan Plateau. *Resour. Sci.* **2019**, *41*, 1093–1101. [[CrossRef](#)]
31. Zhou, L. *Chinese Agricultural Geography*; Science Press: Beijing, China, 2007.
32. Zhang, Y.; Li, B.; Zheng, D. Geographic information system data of the scope and boundary of the Qinghai-Tibet Plateau. *Glob. Chang. Data Wareh.* **2014**. [[CrossRef](#)]
33. Institute of Geographic Sciences and Natural Resources Research, CAS. Earth Observation Data Sharing Plan. Available online: <http://eds.ceode.ac.cn/nuds/freedataquery> (accessed on 30 September 2020).
34. Oreti, L.; Giuliarelli, D.; Tomao, A.; Barbati, A. Object oriented classification for mapping mixed and pure forest stands using very-high resolution imagery. *Remote Sens.* **2021**, *13*, 2508. [[CrossRef](#)]
35. Benz, U.C.; Hofmann, P.; Willhauck, G.; Lingenfelder, I.; Heynen, M. Multi-resolution, object-oriented fuzzy analysis of remote sensing data for GIS-ready information. *ISPRS J. Photogramm. Remote Sens.* **2004**, *58*, 239–258. [[CrossRef](#)]
36. Ma, W. Characteristics of Extreme Precipitation in Qinghai-Tibet Plateau and Estimation of Critical Rainfall for Flood Disasters. Master’s Thesis, Qinghai Normal University, Xining, China, 2019.
37. Chavez, P.S.; Berlin, G.L.; Sowers, L.B. Statistical-method for selecting Landsat MSS Ratios. *J. Appl. Photogr. Eng.* **1982**, *8*, 23–30.
38. *Regulations on Converting Farmland to Forests*; State Council of the People’s Republic of China: Beijing, China, 2002.
39. Jia, W.; Wang, J.; Shi, P.; Ma, W. The progress and prospect of remote sensing monitoring of rocky desert dynamic changes in the ice and snow melting area of the Qinghai-Tibet Plateau. *J. Geo-Inf. Sci.* **2021**. [[CrossRef](#)]
40. Zhang, C.; Tong, L.; Liu, Z.; Qiao, M. Identification method of seed maize plot based on multi-temporal GF-1 WFV and Kompsat-3 Texture. *J. Agric. Mach.* **2019**, *50*, 163–168. [[CrossRef](#)]
41. Zhang, H.; Tian, T.; Zhang, Q.; Lu, Z. Study on Extraction of Paddy Rice planting area in low fragmented regions based on GF-1 WFV images. *Remote Sens. Technol. Appl.* **2019**, *34*, 785–792. [[CrossRef](#)]